On the fatigue life enhancement due to periodic healing of a NiTi shape memory alloy

Author links open overlay panel V.V. Shastry [a], Gaurav Singh [b], U. Ramamurty [c d]

[a]

[a] Kellogg School of Management, Northwestern University, 2211 Campus Drive, Evanston, IL, 60208, United States
[b] 403, LS Building, Sanjaynagar, Bangalore, 560090, India
[c] School of Mechanical and Aerospace Engineering, Nanyang Technological University, 639798, Singapore
[d] Institute of Materials Research and Engineering, Agency for Science, Technology and Research (A∗STAR), 138634, Singapore

Abstract

Fatigue failure in NiTi based shape memory alloys (SMAs) that are in the austenitic state is accelerated by the progressive accumulation of stress-induced martensite (SIM) under cyclic loading, even when the maximum stress of the fatigue cycle is well below that required for stress-induced martensitic transformation. Wagner et al. (2008) [1] have shown that periodic annealing of the fatigued specimens at temperatures well above the austenitic finish temperature, which they termed as 'healing', can enhance the fatigue life of the SMAs that are cyclically loaded in the austenitic state. In this paper, the optimum interval at which healing must be performed is investigated. Experimental results show that considerable improvement in the total life of the SMA component can be realized if the fatigued specimens are healed periodically right after 20% of their service life has lapsed. Healing later (at 40% and 60% of the fatigue life) does not lead to any significant improvement, indicating that irreversible damage has already set in. Real-time infrared thermography technique was used to study the thermal signatures during tensile and fatigue testing. Results show that it is possible to monitor the formation of SIM during cyclic loading using thermography.

Keywords

Shape memory alloy; Martensite; Austenite; Infrared thermography; Fatigue

1. Introduction

Shape memory alloys (SMAs) are susceptible to 'structural' and 'functional' fatigue when subjected to cyclic loading [[2], [3], [4], [5], [6], [7], [8], [9]]. Structural fatigue refers to accumulation of damage at the microstructural scale, leading to crack nucleation, growth, and eventual fracture of the component. On the other hand, functional fatigue refers to the progressive loss of the functional properties such as degradation of the damping capacity, irreversible changes in the phase transformation temperatures as well as the stress levels at which they occur (for stress-induced phase transformations), and a progressive reduction in the recoverable (pseudo-elastic) strains [2,7,8]. Both these aspects of fatigue in SMAs, which are often coupled, have been widely studied [[2], [3], [4], [5], [6], [7], [8]]. For SMAs that are in the austenitic state (i.e., the testing temperature is above the alloy's austenitic finish temperature, A_f), progressive stabilization of martensite with mechanical cycling, which is aided by the dislocation accumulation, occurs even when the maximum stress of the fatigue cycle is well below the stress required for the austenite to martensite transformation at that testing temperature. In view of this, many different approaches to enhance the fatigue performance were explored. It was shown that thermal cycling of a NiTiFe SMA can 'homogenize' the accumulated strain, which, in turn, can enhance the fatigue life by 200–500% as compared to that of the solubilized specimens [10]. Periodic heating the fatigued SMA samples to above A_f was also found to decrease the functional property degradation via the reversion of the accumulated martensite [1,[11], [12], [13]]. A preliminary investigation conducted by Wagner et al. [1] has shown that such a 'healing' heat treatment has the potential to enhance the fatigue life of NiTi SMAs. However, a systematic study that illustrates as to when such interventions are most optimal has not been performed yet. For example, it would be reasonable to assume that the healing would only work if it is done before the nucleation of a dominant crack occurs under cyclic loading conditions [1]. On the other hand, healing right after the SMA component was in service for a small fraction of the estimated fatigue life might not be also optimal. Keeping this in view, a systematic experimental study was conducted in this work so as to examine as to when the 'healing' intervention can enhance the fatigue life of the SMA the best.

An additional objective of the present study is to examine the utility of infrared (IR) thermography, which is a non-destructive, real-time and non-contact technique, in detecting early region of failure during testing. Due to its high thermal resolution and high frame capture rates [14], it is particularly suitable to observe the thermal signatures of SMAs during tensile and fatigue loading. Earlier studies used IR thermography to observe dynamic temperature distribution in SMA surgical staples as a function of laser pulse parameters to optimize closure of surgical staples [15] and local changes of the phase transformation in NiTi SMAs [[16], [17], [18], [19]]. More recently, evidence of reverse transformation to austenite close to cracks in NiTi SMAs [20] and the phenomenon of temperature and stress oscillations under cyclic phase transition of a nano-structured polycrystalline NiTi strip were also studied [21].

However, the utility of IR thermography for understanding the thermal signatures of various processes during tensile and fatigue testing of SMAs has not been explored yet.

2. Material and experiments

A 15 kg batch of $Ni_{50.6}Ti_{49.4}$ (in at.%) alloy was made by vacuum induction melting appropriate amounts of pure Ni and commercially pure Ti in a graphite crucible and then casting into cylindrical ingots of 70 mm diameter. The ingots were then vacuum arc re-melted and cast into ingots of 110 mm diameter, which were then hot forged at 900 °C into rectangular blocks of 50 x 100 mm^2 cross section. They were subsequently hot rolled at 900 °C into 15 mm thick slabs and finally solutionized at 850 °C for 1 h. Flat dog bone shaped specimens with 6 mm width, 2 mm thickness, and 25 mm gage length were electro-discharge machined from the slabs. A schematic drawing of the specimen used for tensile and fatigue testing is shown in Fig. S1(a) of the supplementary information (SI). To impart pseudo-elasticity (PE) and to erase any history associated with the thermo-mechanical processing and machining, test specimens were solutionized at 800 °C for 30 min and then air-quenched, followed by annealing at 500 °C for 30 min and then furnace cooled. All the test specimens were vacuum sealed in quartz tubes during solutionizing and annealing heat treatments. The martensitic finish, martensitic start, austenitic start, and austenitic finish temperatures (M_f, M_s, A_s, and A_f, respectively) of the NiTi SMA in the annealed condition were determined as −2.8, 3.4, 3.1, and 10.5 °C, respectively, using differential scanning calorimetry (DSC) with the heating and cooling rates of 10 °C/min between −20 and 50 °C. Fig. 1 shows a representative DSC scan of the NiTi SMA examined in this study. The alloy exhibits a one-step phase transformation both during heating and cooling in the investigated temperature range. Since the alloy's A_f is 10.5 °C, it is austenitic at room temperature (~23 °C). The obtained values of martensitic transformation temperatures in the present work are consistent with those reported by Nayan et al. [22], who recorded M_f = −21.4 °C, M_s = 2.1 °C, A_s = −1.3 °C and A_f = 23.4 °C in a $Ni_{50.3}Ti_{49.7}$ (at.%) SMA that has a similar processing route as that used in the present study. An increase in the Ni content by ~0.3 at.% in the alloy used in the present work results in the stabilization of martensite phase [23] by increasing M_s from 2.1 to 3.4 °C and reducing M_f from −21.4 to −2.8 °C.

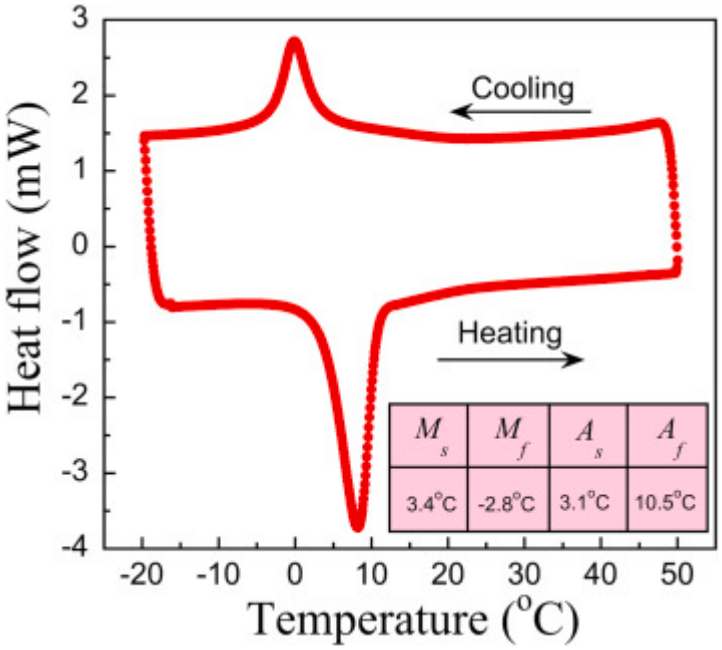

1. Download: Download high-res image (285KB)
2. Download: Download full-size image

Fig. 1. Representative DSC scan of the austenitic NiTi shape memory alloy in the as-annealed condition. Various transformation temperatures measured from such scans are listed in the inset table.

Tensile and unnotched fatigue tests were performed in a servo-hydraulic testing machine equipped with a data acquisition system and hydraulic grips. A schematic drawing of the experimental set-up is shown in Fig. S1(b). An extensometer with a gage length of 25 mm, fastened to the sample, was used for measuring the strain for both tensile and fatigue tests. Care was taken to avoid slippage of extensometer during testing. Tensile tests were conducted at room temperature (~23 °C), at a strain rate of 10^{-3} s^{-1}. Tension-tension fatigue tests were performed at a frequency f 0.5 Hz and stress ratio, R = 0.1. The test frequency was low enough to prevent self-heating of the samples during cyclic loading. Fatigue tests were performed in the load-controlled mode at two fixed stress ranges, $\Delta\sigma$ (= σ_{max} - σ_{min}) of 225 and 275 MPa. All the fatigue tests were conducted at room temperature (~23 °C) using the sinusoidal loading waveform.

During the tensile and fatigue tests, an IR camera (VarioCAM) was used to continuously monitor (and record) the temperature of the specimen surface, which has been highlighted in red in Fig. S1(a). Thermographic data such as maximum (T_{max}), minimum (T_{min}) and mean (T_{mean}) temperatures during each fatigue cycle were recorded during the tests in real time on the specimen surface at a given frame. The key technical characteristics of the IR camera are as following: maximum picture size - 640 x 480 pixels, operating spectral range - 7.5–15 µm, measurement accuracy - ±1 °C, temperature resolution - 0.03 °C at room temperature, and lateral resolution ~ 100 µm. The infrared camera was located at ~300 mm from the testing machine in all

the cases. For avoiding viewing angle effects, the camera axis was oriented perpendicular to the test specimen surface. Constant ambient temperature (~23 °C) and humidity was maintained during the experiments. Thermal images were continuously acquired at a frame capture rate of 1 Hz for majority of the test duration and was increased to 5 Hz close to failure. Real-time tensile stress (σ) vs. tensile strain (ε) and temperature (T) vs. time (t) data were monitored and recorded digitally until failure of the specimens. Post testing, all the IR thermographic data was analyzed using a commercial software package.

Uninterrupted fatigue tests were first performed at the selected stress ranges ($\Delta\sigma$) of 225 or 275 MPa, to determine the number of cycles to failure (N_f) in the absence of any healing interventions. The load ratio (R) during cyclic loading was always maintained at 0.1. Note that the maximum stresses of the fatigue cycles (σ_{max}), which are about 250 and 305 MPa for the two stress ranges utilized, are well within the elastic limit of the SMA investigated. First, the fatigue lives with no healing interruption ($N_{f,NH}$) at the two $\Delta\sigma$ levels were determined. Subsequently, fatigue testing on samples was interrupted after a predetermined number of cycles (N), which corresponds to either 0.2, 0.4 or 0.6 $N_{f,NH}$. The HHT process involves interrupting the fatigue test after a predetermined number of fatigue cycles, taking the specimen out of the testing frame, immersing the specimen in an oil bath that was maintained at a temperature of 60 °C (which is sufficiently well above A_f) for 300 s, and then allowing it to attain thermal equilibrium with the ambient temperature by air cooling, before continuing with the fatigue testing. Various HHT intervals examined in the present work and their acronyms are listed in Table 1. For example, $N_{f,HT0.2,0.4}$ refers to number of cycles to failure of the fatigue specimens that were subjected to healing after being subjected to stress cycles that correspond to 0.2 and 0.4 of the corresponding $N_{f,NH}$. For a given condition and stress range, three tests were performed.

Table 1. Fatigue lives of the austenitic NiTi SMA tested with different HHT intervals.

Acronym	**Cumulative healing intervals**	**Average number of cycles to failure, N_f**		**Enhancement in cycles to failure due to healing, ΔN_f**	
		$\Delta\sigma$ = 225 MPa	**$\Delta\sigma$ = 275 MPa**	**$\Delta\sigma$ = 225 MPa**	**$\Delta\sigma$ = 275 MPa**
$N_{f,NH}$	None	4108 (4189, 4119, 4016)	1960 (1789, 1980, 2140)	NA	NA
$N_{f,HT0.2}$	800 ($\Delta\sigma$ = 225 MPa) 400 ($\Delta\sigma$ = 275 MPa)	5346 (5318, 5582, 5137)	2438 (2509, 2281, 2525)	1238	478
$N_{f,HT0.2,0.4}$	800&1600 ($\Delta\sigma$ = 225 MPa) 400&800 ($\Delta\sigma$ = 275 MPa)	5352 (5156, 5114, 5786)	2632 (2413, 2509, 2973)	1244	672

Acronym	Cumulative healing intervals	Average number of cycles to failure, N_f		Enhancement in cycles to failure due to healing, ΔN_f	
		Δσ = 225 MPa	**Δσ = 275 MPa**	**Δσ = 225 MPa**	**Δσ = 275 MPa**
$N_{f,HT0.2,0.4,06}$	800&1600&2400 (Δσ = 225 MPa) 400&800&1200 (Δσ = 275 MPa)	6622 (6278, 7326, 6262)	2783 (2690, 2454, 3204)	2514	823
$N_{f,HT0.4}$	1600 (Δσ = 225 MPa) 800 (Δσ = 275 MPa)	4908 (4933, 4672, 5120)	2362 (2442, 2121, 2522)	800	402
$N_{f,HT0.6}$	2400 (Δσ = 225 MPa) 1200 (Δσ = 275 MPa)	4362 (4532, 4352, 4202)	1925 (1862, 1760, 2153)	254	−35

The thermographic signature of an austenitic NiTi SMA during tensile testing can differ significantly from those of regular metallic alloys due to the stress-induced martensitic transformation (SIMT) in the SMA. For example, the commonly observed stress plateau in the quasi-static σ vs. ε response (due to SIMT) of the austenitic SMA [2,24] is absent in the conventional metallic alloys. This can result in different T vs. t characteristics during different stages of tensile testing in comparison to conventional metallic alloys. For comparison purposes, specimens of the Inconel 718 alloy (referred as IN-718 here afterwards) in both the as-cast and heat-treated conditions, with identical specimen geometries and testing conditions, were tested. The reasons behind selecting IN-718 are that (a) it is commercially available readily and (b) the Ni content in NiTi SMA and IN-718 is approximately similar ~50 at.% Ni.

3. Results and discussion

3.1. Quasi-static tensile stress-strain responses

Fig. 2 shows the quasi-static engineering stress vs. engineering strain responses for the austenitic NiTi SMA in tension. While some of the tensile specimens were unloaded after ~3.1% engineering strain to examine the PE characteristics of the SMA under investigation, others were loaded continuously until failure. Following the initial linear elastic regime, inelastic strain accumulates at nearly-constant stress due to SIMT, which begins at a stress, σSAM, of 375 MPa and finishes at σFAM= 400 MPa with a total transformation strain of 2.5% (εfAM−εSAM) [25]. When the sample is unloaded after a tensile strain ε of ~3.1%, the reverse transformation from martensite to austenite occurs. Excellent PE was observed with the stress-strain responses showing reproducibility over five load-unload cycles with no residual strain. When loaded continuously to failure, the SIMT regime is followed by the elastic deformation of the martensite until it yields [26,27], which is immediately followed by the specimen failure at a stress of ~1050 MPa with a corresponding failure strain of ε ~7.3%.

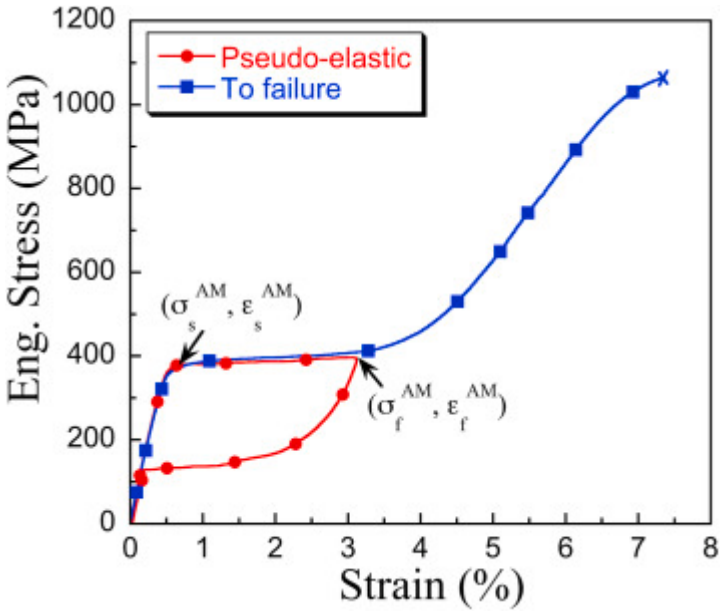

1. Download: Download high-res image (266KB)
2. Download: Download full-size image

Fig. 2. Engineering stress vs. strain responses of the austenitic NiTi shape memory alloy. The red curve, which was obtained by unloading after deforming the SMA to ~3.1% engineering strain, illustrates its pseudo-elastic behavior. The blue curve is obtained by continuous loading of the tensile specimen to failure. (For interpretation of the references to colour in this figure legend, the reader is referred to the Web version of this article.)

The engineering stress-strain responses of the IN-718 alloy in the as-cast and heat-treated conditions are displayed as Fig. S2 in SI. The stress levels for IN-718 alloy in the heat-treated condition was significantly higher in comparison to the as-cast condition. This was mainly attributed to precipitation hardening from the γ'/γ" precipitates formed during ageing heat-treatment [28]. While IN-718 in the as-cast condition showed significant strain-hardening, it was limited in the heat-treated condition before failure. Specimens of IN-718 in the as-cast condition did not fail even though they were loaded until ε ~35%, whereupon the tests were stopped as the maximum extension limit of the machine was reached.

Figs. 3 and S3 show the variations of engineering stress and (a) T_{mean} and (b) T_{max} with *t*, recorded using thermographic measurements for NiTi SMA and IN-718, respectively. In these figures, open symbols refer to σ while filled symbols refer to T_{mean}/T_{max}. From these plots, the distinct tensile and thermal characteristics of the two materials can be seen. In the SMA, both T_{mean} and T_{max} continuously increase, but in a nonlinear fashion with *t*, up to the end of the PE regime. If the sample was unloaded at the end of this regime (as in Fig. 2), a precipitous drop in both the temperatures was observed. If, on the other hand, the specimen is continuously loaded beyond PE (to failure), both T_{mean} and T_{max} reduce gradually from the peak, before attaining the steady state values of 23.5 and 24 °C, respectively, at $t > 800$ s. A steep increase in T_{max} (by ~4 °C) was noted when the specimen fails, the increase in T_{mean} is comparatively insignificant (~1 °C). For the IN-718 alloy in as-cast and heat-treated conditions (Fig. S3), the variations in both T_{mean} and T_{max} with *t* were marginal and gradual during the elastic deformation regime and up to elastic-to-plastic transition. Post yielding, a gradual rise in both T_{mean} and T_{max} was observed, which contrasts with the thermal signature observed during the deformation of NiTi SMA, where both T_{mean} and T_{max} gradually decrease before stabilizing with steep increase in T_{max} at failure. Both T_{mean} and T_{max} increase in a marked manner in IN-718 close to failure in the heat-treated condition; such a thermal signature was absent in as-cast condition as test was interrupted before specimen could reach necking or failure.

During tensile deformation of metallic alloys like IN-718, plastic work done is thermodynamically irreversible and a large fraction (~95%) of the total mechanical work is dissipated as heat while the remaining work is expended for microstructural changes [29]. This causes continuous increase in the specimen temperature in the work-hardening regime due to plastic deformation prior to necking, which is consistent with the observations made from Fig. S3. The observed temperature increase in the neck region prior to failure is due to localized plastic deformation. In the elastic and elastic-to-plastic transition regimes, the extent of plastic deformation is limited with little or no rise in T_{mean} and T_{max}. Moreover, as the tensile tests are performed at a low strain rate (10^{-3} s^{-1}) sufficient time is available for the generated heat to dissipate through the specimen surface to the surrounding. This was further confirmed by the measured values of T_{mean} and T_{max} which are in the range of ~24–26 °C in the elastic and elastic-to-plastic transition regimes.

The gradual increase in T_{mean} and T_{max} with *t* during the PE regime of the NiTi SMA is related to SIMT and is consistent with the findings of Gadaj et al. [30]. In their work, tensile testing on an austenitic NiTi SMA in sheet form was performed in the temperature range 22–80 °C and the evolution of temperature on the specimen surface was also monitored using the IR thermography technique. It was found that during loading portion of the stress-strain response, SIMT is always accompanied by an increase in temperature while temperature decreases during unloading due to the reverse transformation from martensite to austenite. Similarly, in the present study, the NiTi SMA is nearly-completely martensitic at the end of PE, and reverse transformation from martensite to austenite during unloading results in a decrease of both T_{mean} and T_{max} (Fig. 3). Beyond SIMT, when loaded to failure, elastic deformation of the martensite phase results in gradual decrease of T_{mean} and T_{max}, and the observed temperature plateau is due to the attainment of a thermal equilibrium between the deforming specimen and the surroundings.

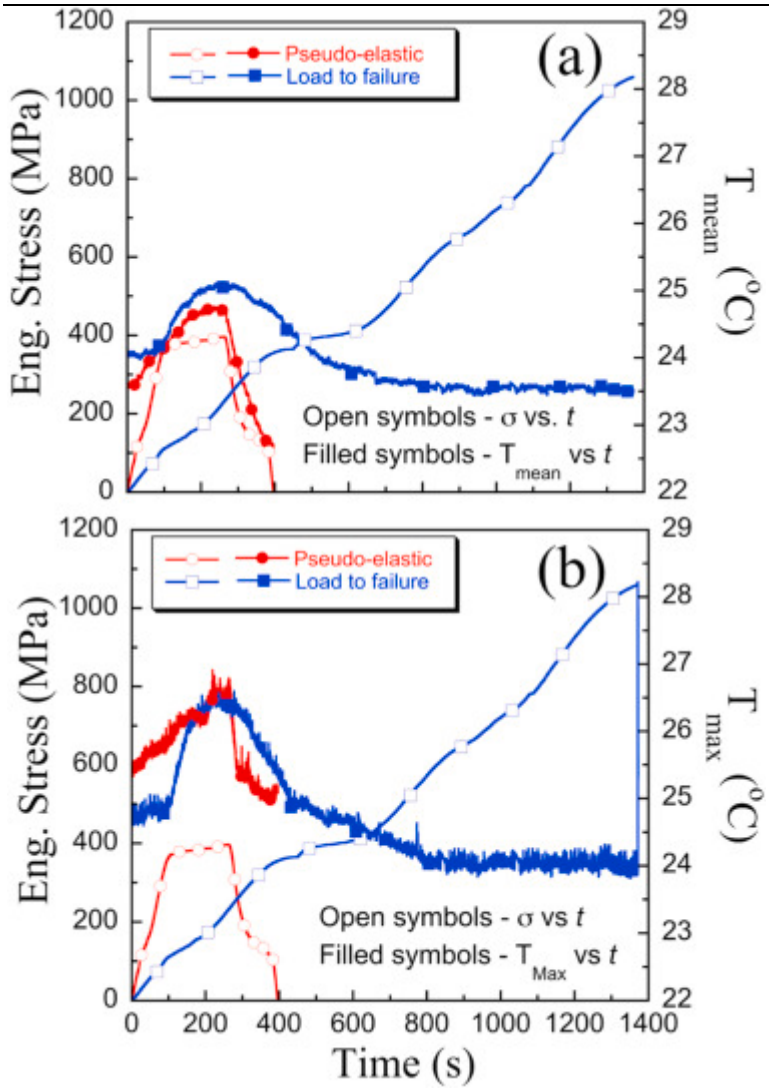

1. Download: Download high-res image (527KB)
2. Download: Download full-size image

Fig. 3. The variations of engineering stress and (a) the mean temperature (T_{mean}) and (b) the maximum temperature (T_{max}) with time, recorded by the real-time thermographic measurements on the tensile specimens of the NiTi shape memory alloy in pseudo-elastic and load to failure conditions.

3.2. Effect of HHT on the fatigue properties

The measured fatigue lives of NiTi SMA with and without HHT, cycled at Δσ of 225 and 275 MPa, are summarized in Table 1. In it, both the average values as well as the actual N_f values (which are used for computing the average) are listed. It can be noted from them that the scatter in N_f, in general, is not significant. The average values of $N_{f,NH}$ at Δσ of 225 and 275 MPa are 4108 and 1960. On their basis, 800, 1600, and 2400 cycles, which correspond to ~0.2, 0.4, and $0.6N_{f,NH}$, respectively, were selected for healing interventions on specimens fatigued at Δσ = 225 MPa. The corresponding cycles are 400, 800, and 1200 for specimens fatigued at Δσ = 275 MPa. The observed enhancement in fatigue life, due to healing (ΔN_f), if any, is estimated by subtracting respective $N_{f,NH}$ from the average fatigue lives of the healed specimens and is also listed in Table 1.

From the results obtained, it can be first noted that when healing was performed relatively late in the fatigue life (~$0.6N_{f,NH}$, i.e., after 2400 and 1200 cycles for Δσ = 225 and 275 MPa, respectively), no clear benefit due to healing could be seen as the measured fatigue lives of healed specimens are within the scatter band of the $N_{f,NH}$ data. This observation suggests that irreversible microstructural damage already sets in when the samples are cycled for $0.6N_f$. When healing was performed earlier in the fatigue life than the previous instance, i.e., at ~$0.4N_{f,NH}$ (i.e., after 1600 and 800 cycles for Δσ = 225 and 275 MPa, respectively), some enhancements in the average fatigue life could be observed at both Δσ examined. However, the average enhancements are only about half of the number of cycles used for the healing interval (see Table 1). This observation implies that healing interventions even at ~$0.4N_{f,NH}$ are not necessarily optimal (or early enough). Together, the observations made of specimens healed at 40% and 60% of $N_{f,NH}$ imply that permanent fatigue damage in SMAs could be setting in relatively early as compared to that in regular (or non-transforming) metallic materials. In the latter case, the fraction of the fatigue life that is expended before a dominant fatigue crack nucleates in the nominally defect free unnotched specimens can be as high as 80% [31].

When the first healing treatment was performed at relatively early stage of the fatigue life (corresponding to ~$0.2N_{f,NH}$, i.e., after 800 and 400 cycles for Δσ = 225 and 275 MPa, respectively) and then repeated at the same N intervals, unambiguous accrual of the benefit in terms of enhanced fatigue life could be noted. Data presented in Table 1 indicates that the increment in N_f is more pronounced for the lower of the two Δσ levels investigated. It is also apparent that the net enhancement in N_f often

exceeds the cumulative number of healing cycles, indicating that the periodic healing treatments can delay the fatigue failure substantially. To ascertain that the increased fatigue life is due to healing and not because of interruption of the tests (which were necessary for performing the healing treatment), a fatigue test was performed at $\Delta\sigma$ = 225 MPa with a hold period of 300 s after 800 cycles and then resuming the test till failure. The hold interval is similar to the time it takes to complete one healing round. Here afterwards, this test will be referred as 'Interrupted' for brevity. The obtained fatigue life of the specimen that subjected to such interruption was 4084 cycles, which is within the scatter band of $N_{f,NH}$ measured with $\Delta\sigma$ = 225 MPa (see Table 1). This result confirms that HHT is responsible for the increased fatigue life rather than interruption in the fatigue testing that is necessary for healing.

A comparison of the variations in the maximum accumulated plastic strain due to fatigue, ε_p, with loading cycles in NH and HHT conditions for $\Delta\sigma$ of 225 and 275 MPa is made in Fig. 4(a) and (b), respectively. As expected, the level of ε_p is higher in $\Delta\sigma$ = 275 MPa as compared to that in $\Delta\sigma$ = 225 MPa. In the specimen that was continuously fatigue tested until failure (without any healing or interruptions), ε_p increases steadily with loading cycles until failure of the specimen. In the HHT specimen, ε_p increases with N, interruption in testing for HHT causes a significant drop in ε_p and with the resumption in testing ε_p increases again until it reaches plateau value which is maintained till failure. Nayan et al. [22] have demonstrated that plastic strain accumulation with the loading cycles during fatigue testing of an austenitic NiTi SMA mainly arises from SIMT, which eventually leads to failure. On that basis, we infer that the accumulated plastic strain due to fatigue gets partially relieved during HHT as it transforms the stabilized martensite back to austenite and delays failure. Any elastic strain associated with the austenite phase during fatigue testing at $\Delta\sigma$ = 225 and 275 MPa (which are well below the stress required for inducing SIM under quasi-static loading conditions), will be completely recovered during unloading.

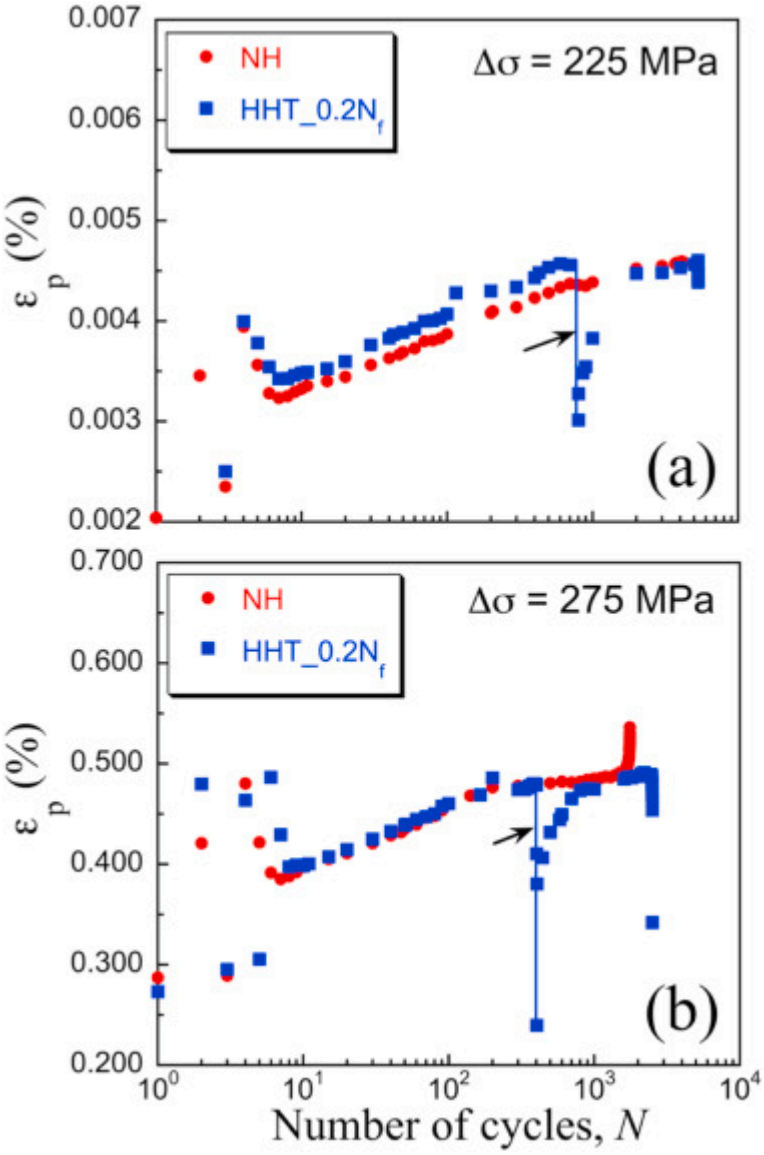

1. Download: Download high-res image (354KB)
2. Download: Download full-size image

Fig. 4. The variation of the maximum plastic strain, ε_p, accumulated with loading cycle in NH and HHT conditions at Δσ of (a) 225 and (b) 275 MPa. The healing heat treatments (HHT) performed at 800 and 400 cycles in (a) and (b) are highlighted with arrows.

Fig. 5(a) and (b) show the variations of the stress-strain hysteresis loop areas, ΔH, with loading cycles in NH and HHT conditions at Δσ of 225 and 275 MPa, respectively. For comparison, variation of ΔH in the 'Interrupted' test performed at Δσ = 225 MPa is also shown in Fig. 5(c). Unlike ε_p, ΔH increases sigmoidally with N, viz. with an initial low-sloped portion followed by a region with higher slope and subsequent saturation. The saturation in ΔH occurs at about ~$0.2N_f$ (~800 and 400 cycles at Δσ = 225 and 275 MPa, respectively), as seen in both Fig. 5 (a) and (b). Upon performing HHT, the area of the hysteresis loop takes significantly longer ~4600 and 1800 cycles at Δσ = 225 and 275 MPa, respectively, to reach saturation levels again, possibly due to

reverse transformation to austenite due to HHT. On the other hand, in the 'Interrupted' test (Fig. 5(c)), ΔH increased to the earlier level (prior to hold period) in the same 300–400 cycle window as opposed to ~4600 and 1800 cycles in $N_{f,HT0.2}$ condition, with no noticeable increase in fatigue life due to the interruption as already mentioned. It is important to mention that ε_p vs. N and ΔH vs. N plots in Fig. 4, Fig. 5 are plotted on a log-linear plot.

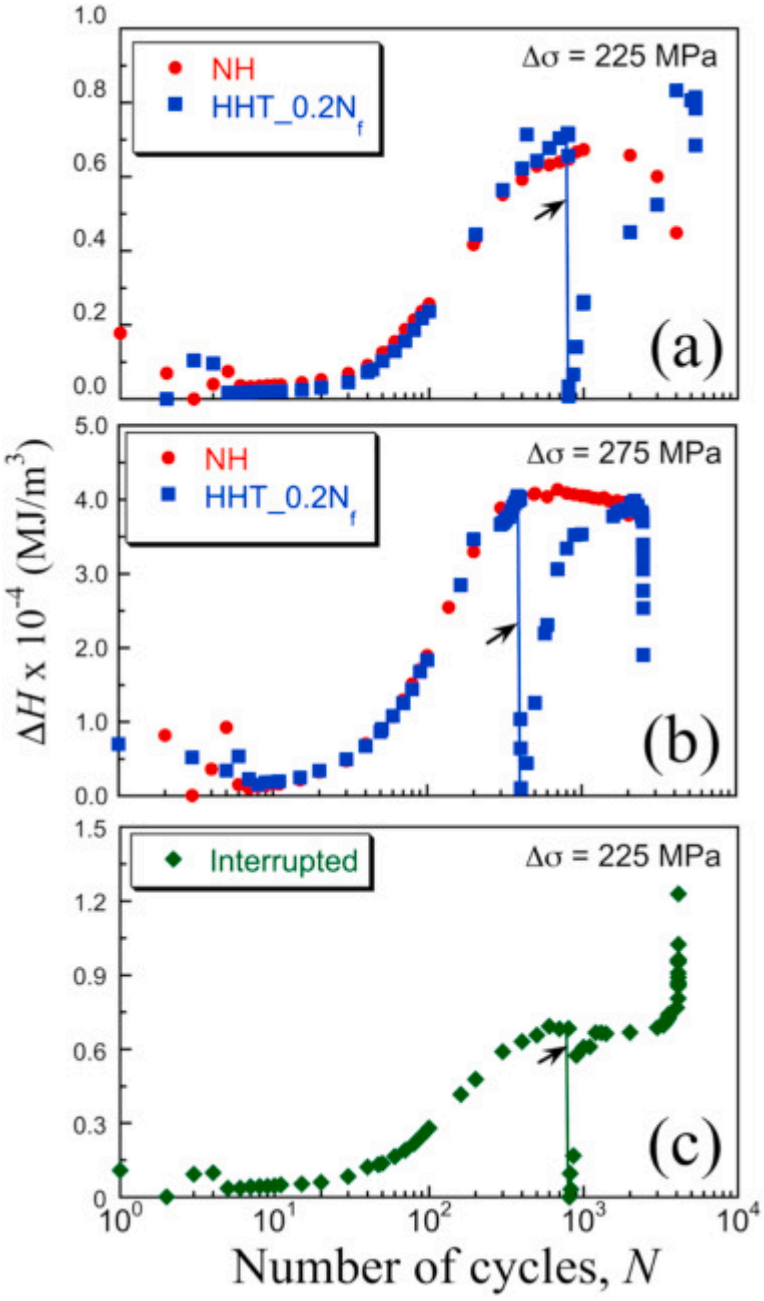

1. Download: Download high-res image (421KB)
2. Download: Download full-size image

Fig. 5. Variations of the stress-strain hysteresis loop areas in NH and HHT conditions in fatigue tests conducted at Δσ of (a) 225 and (b) 275 MPa. HHT was performed at 800 and 400 cycles in (a) and (b), respectively, and is shown with arrows. (c) Area of

the stress-strain hysteresis loop in the 'Interrupted' test conducted at $\Delta\sigma$ = 225 MPa. The arrow in (c) indicates test interrupted at 800 cycles for 300 s without any HHT.

3.3. Thermographic observations

With the baseline thermographic data for the loading, unloading, and failure of the NiTi SMA in place, real-time thermographic measurements were performed during fatigue testing of NiTi SMA samples. Fig. S4 shows the variation of T_{mean} vs. *t* at different frame capture rates of 1 and 5 Hz. The hysteresis of T_{mean} increases from ~0.35 to ~0.6 °C with the increase in frame capture rate from 1 to 5 Hz. However, the instantaneous fluctuation of T_{mean} still aligns itself with the frequency of testing, f = 0.5 Hz, as seen by the 2 s gap between any two successive peaks/valleys. This means that the high thermal resolution of the IR camera is still capable of capturing thermographic signature associated with SIMT during loading and the reverse transformation during unloading even at lower frame capture rate of 1 Hz. However, the difference in temperature levels at each peak and valley might not be represented commensurately at lower frame capture rate but instead, at a fraction of ~60% of the original difference.

To examine the effect of position on the specimen surface (within gage length) on the thermographic data, the highlighted region in red in Fig. S1(a) on which temperature is measured in real time using IR thermography technique is analyzed further by dividing this area into three equal parts: Top third, Middle third and Bottom third. From the acquired IR images at a given frame, these areas of interest analyzed for T_{mean}, T_{max}, and T_{min} in them. Fig. S5 shows the variations of T_{mean} with *t* in them. It appears that T_{mean} depends on the position in the gage length with respect to the actuator of the servo-hydraulic machine. Since the actuator is located at the bottom, see Fig. S1(b), T_{mean} was highest at regions closest to the bottom since it would get stretched first i.e. closest to the actuator. However, the spatial variation in T_{mean} did not cause any discernible difference between the conduction of heat throughout the sample --the entire sample showed a hysteresis of T_{mean}, albeit at slightly different levels at the test frequency of f = 0.5 Hz. Thus, within the gauge length the hottest regions are most likely to be near the bottom parts and the coldest at the top.

Typical thermal images showing temperature evolution near failure during (a) unloading and (b) loading of a HHT specimen subjected to $\Delta\sigma$ = 275 MPa are shown in Fig. 6(a) and (b), respectively. The thermal image of the specimen at failure is also shown in Fig. 6(c). Corresponding video can be found in the SI file. The temperature field evolution is different during the unloading and the loading parts of the fatigue cycle with the temperature at the surface of the specimen being higher in latter. It can also be seen that fracture occurs at the Middle third area of the gauge length. Close to failure, several "hotspots" are formed, as seen in Fig. 6(b), which are hotter than their surroundings at every cycle. These regions correspond to SIMT, which has stabilized

after many fatigue cycles and where eventual fracture was observed to occur. This observation indicates that IR thermography technique is capable of prior indication of the region of failure during fatigue testing. Fig. 7 is the representative plot of T_{max} and T_{mean} in the "soon to fail" Middle third region of the gauge length. In comparison to the Middle third region where failure will occur – extreme temperature zones - Bottom third could be expected to be the hottest region and the Top third could be expected to be the coldest region in the gauge length of the sample. Hence, an indicator of the "hotness", T_{max} readings from the Bottom third and the "coldness", T_{min} readings from the Top third are contrasted in Fig. S6 with the magnitudes of T_{max} and T_{min} from the "soon to fail" Middle third region of the gage length. It can be seen from Figs. 7 and S6 that specimen has failed in the Middle third region of the gauge length at t ~ 6238 s with T_{max} value of ~24.9 °C. One may argue that SIM formation at the hotspot location with T_{max} ~ 24.9 °C is within experimental range of variation of room temperature (~23 °C). However, the high temperature resolution of the IR camera (~0.03 °C) easily distinguishes temperature rise associated with SIM formation (red region in Fig. 6(b)) with green-yellowish regions associated with austenite phase. Moreover, the fatigue test frequency utilized (0.5 Hz) is not too small to conduct heat away from the hotspot formation location to the surrounding and make the specimen surface temperature uniform ~23 °C (room temperature), which is not observed.

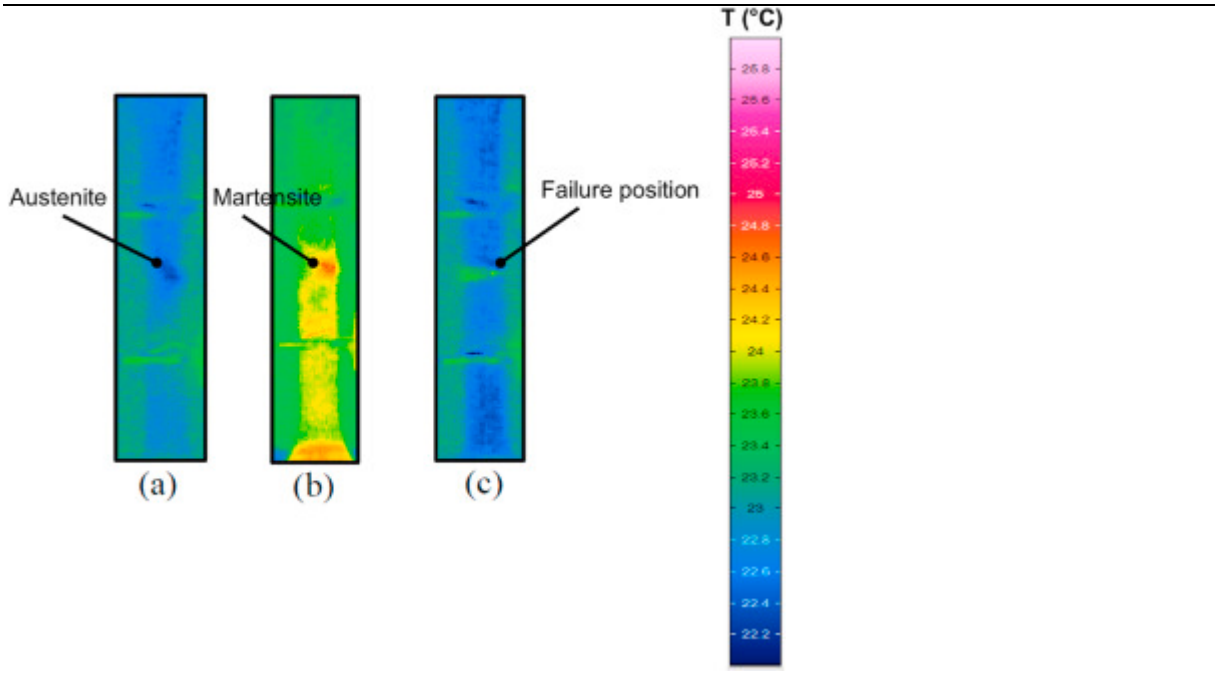

1. Download: Download high-res image (336KB)
2. Download: Download full-size image

Fig. 6. Representative thermal images obtained during fatigue testing at $\Delta\sigma$ = 275 MPa of HHT specimen near failure during (a) unloading and (b) loading part of the fatigue cycle. (c) Thermal image at failure. Color code for temperature is shown in the right side of the figure. Temperature and lateral resolutions of the IR camera are 0.03 °C and ~ 100 μm, respectively. (For interpretation of the references to colour in this figure legend, the reader is referred to the Web version of this article.)

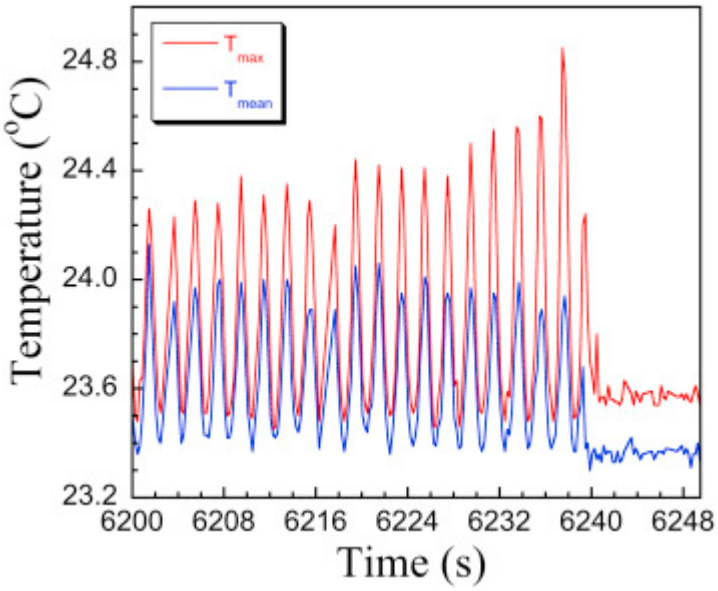

1. Download: Download high-res image (442KB)
2. Download: Download full-size image

Fig. 7. Variations of the mean and maximum temperatures (T_{mean} and T_{max}, respectively) with time (t) in the middle third region of the gauge length.

Figs. S7 (a)–(c) show the corresponding thermal maps for the whole experimental setup. It can be seen in Fig. S7 that the extremes of the temperature have shifted from the terminal ends of the gage length to the Middle third region, where, presumably, failure is due to occur (Fig. S7b). In Fig. 6(c), it can be seen that failure has begun at the region of hotspot formation and then spread to the left, thus breaking the sample into two pieces. This local effect of thermal cycling, where the hot zone is due to the thermal signature of exothermic SIM formation while the cold regions (in the neighborhood, as seen Fig. 6(a)) indicate the reverse transformation. This behavior was also observed during crack extension in NiTi SMAs [20], where, martensite was found to form in front of the crack tip upon application of a tensile stress. But the affected zone undergoes reverse transformation to austenite upon unloading. Their study also used thermographic methods to observe a scenario where a crack grew into SIM microstructure, which reverse transforms into to austenite in the crack-wake.

Possible reasons behind the observed beneficial effects of HHT were also studied with the help of thermographic measurements. Fig. 8 compares the variation of real-time T_{mean} with t in HHT and Interrupted conditions. The hysteresis of T_{mean} is quite steady in both the cases. However, the magnitude of T_{mean} decreases after resumption in fatigue loading after HHT at 800 cycles for 300 s. On the other hand, in the Interrupted test, the hold period at 300 s without HHT showed no change in T_{mean} upon resumption of testing. This further supports the hypothesis that HHT increases fatigue life by reverse transforming the stabilized martensite (that occurs due to fatigue loading) to austenite and thus delays failure. A similar trend was observed in the case

of T_{max} also, which is an indicator of the success of HHT in reverse transforming the entire sample to austenite.

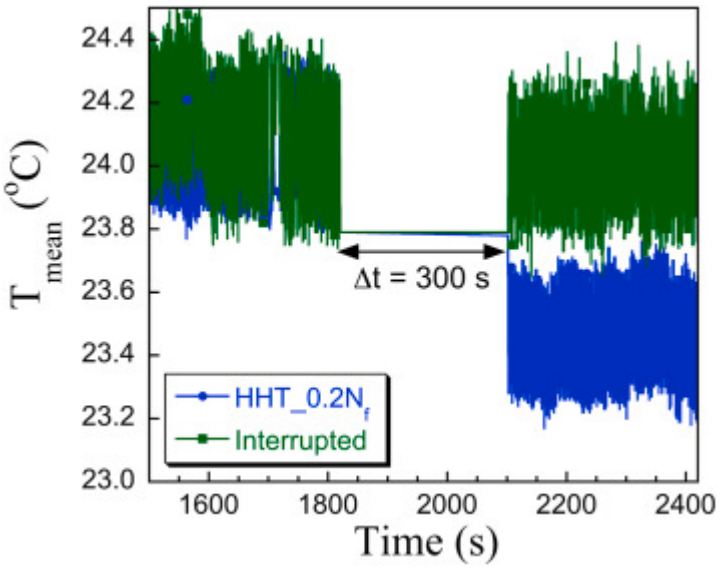

1. Download: Download high-res image (300KB)
2. Download: Download full-size image

Fig. 8. The variation of T_{mean} with *t* in HHT and Interrupted fatigue tests.

4. Summary and conclusions

In this study, the possibility of enhancing the fatigue life of an austenitic NiTi shape memory alloy cyclically loaded at room temperature via periodic healing heat treatment was examined systematically. This was coupled with real-time infrared thermographic measurements to ascertain thermal signatures during tensile and fatigue testing. Following main conclusions are drawn from this work:

(1) The fatigue life of an austenitic NiTi SMA, in which cyclic loading causes the stabilization of the martensite, can be improved substantially (by up to 61%) through periodic healing treatments that involve heating the fatigued specimen to temperatures above its austenite finish temperature and annealing to revert the stabilized martensite into austenite. Healing is particularly beneficial when performed early in service (at about 20% of the fatigue life estimated with continuous testing until failure). From the practical feasibility standpoint of view, it should be possible to perform healing quite easily in actual service conditions. Localized heating methods like laser, electromagnetic induction, infrared (IR) techniques can be used [[32], [33], [34], [35]], which can avoid service life disruption of the component along with improved fatigue life. This is particularly true for majority of the applications of NiTi SMAs which are used in very small forms like wires, tubes etc. where localized heating is practically feasible due to the small size of the component.

(2) Thermal imaging of the fatigue specimens showed several “hotspots” on the specimen surface close to failure, which are signatures of martensite that has stabilized after many fatigue cycles and where eventually fracture occurred. It was found that IR thermography technique is capable of prior indication of the region of failure during fatigue testing.

Data availability

Experimental data presented in this work including data used in figures and supplementary information file is available upon request.

CRediT authorship contribution statement

V.V. Shastry: Conceptualization, performed experiments, Writing – original draft, Data curation, reviewing and editing. **Gaurav Singh:** Writing - reviewing, Data plotting and editing. **U. Ramamurty:** Conceptualization, Funding acquisition, Supervision, draft reviewing and editing.

Declaration of competing interest

The authors declare that they have no known competing financial interests or personal relationships that could have appeared to influence the work reported in this paper.

Acknowledgements

We are thankful to Mr. Chandru Fernando and Mr. Vijay Petley of the Gas Turbine Research Establishment, Bangalore, India for their kind assistance in the tensile and fatigue experiments reported in this work. The work at the Nanyang Technological University was supported by the funding from Agency for Science, Technology, and Research (A*STAR) via the Structural Metals and Alloys Programme (No. A18B1b0061).

Appendix A. Supplementary data

Download all supplementary files included with this article

What's this?

The following are the Supplementary data to this article:

Media player

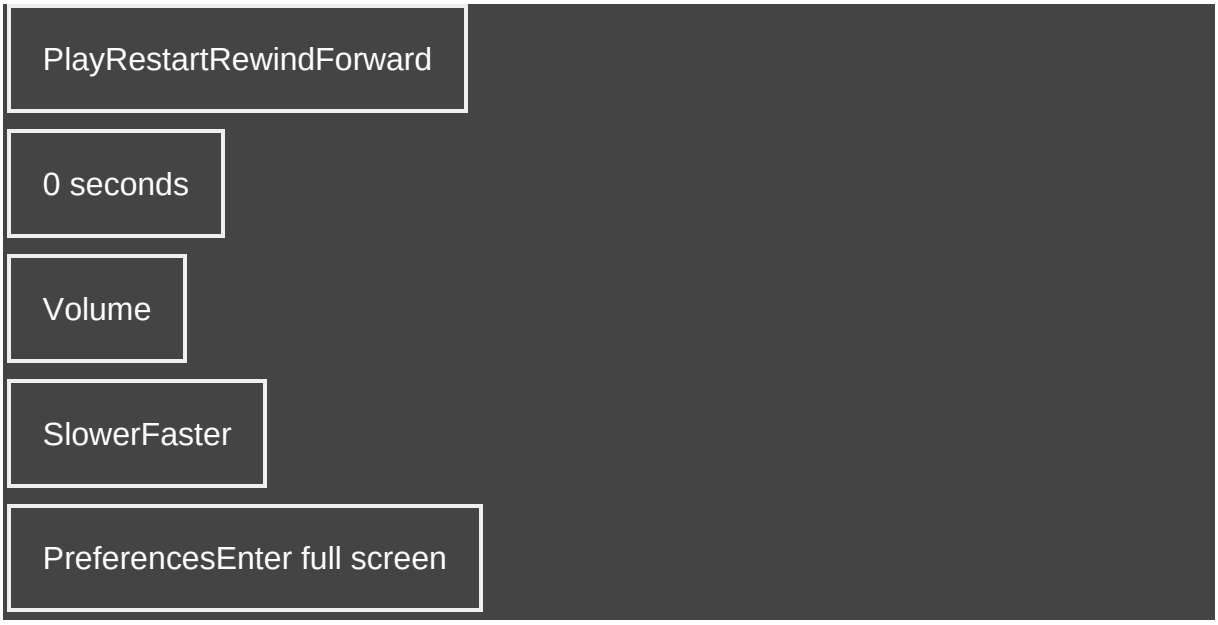

Download: Download video (48MB)

Multimedia component 1.

Download: Download Word document (9MB)

Multimedia component 2.

References

[1]

M.F.X. Wagner, N. Nayan, U. Ramamurty

Healing of fatigue damage in NiTi shape memory alloys

J. Phys. D Appl. Phys., 41 (2008), p. 185408

View at publisherCrossrefView in ScopusGoogle Scholar

[2]

M.J. Mahtabi, N. Shamsaei, M.R. Mitchell

Fatigue of Nitinol: the state-of-the-art and ongoing challenges

J. Mech. Behav. Biomed. Mater., 50 (2015), pp. 228-254

View PDFView articleView in ScopusGoogle Scholar

[3]

G.S. Mammano, E. Dragoni

Functional fatigue of shape memory wires under constant-stress and constant-strain loading conditions

Procedia Eng., 10 (2011), pp. 3692-3707

View PDFView articleGoogle Scholar

[4]

M.J. Mahtabi, N. Shamsaei, M.H. Elahinia

Fatigue of Shape Memory Alloys

Shape Mem. Alloy Actuators. John, New York (2015), pp. 155-190

CrossrefView in ScopusGoogle Scholar

[5]

C. Schmidt, K. Neuking, G. Eggeler

Functional fatigue of shape memory polymers

Adv. Eng. Mater., 10 (2008), pp. 922-927

CrossrefView in ScopusGoogle Scholar

[6]

Y. Gao, L. Casalena, M.L. Bowers, R.D. Noebe, M.J. Mills, Y. Wang

An origin of functional fatigue of shape memory alloys

Acta Mater., 126 (2017), pp. 389-400

View PDFView articleView in ScopusGoogle Scholar

[7]

S. Miyazaki, K. Mizukoshi, T. Ueki, T. Sakuma, Y. Liu

Fatigue life of Ti–50 at.% Ni and Ti–40Ni–10Cu (at.%) shape memory alloy wires

Mater. Sci. Eng., 273 (1999), pp. 658-663

View PDFView articleView in ScopusGoogle Scholar

[8]

G. Eggeler, E. Hornbogen, A. Yawny, A. Heckmann, M. Wagner

Structural and functional fatigue of NiTi shape memory alloys

Mater. Sci. Eng., 378 (2004), pp. 24-33

View PDFView articleView in ScopusGoogle Scholar

[9]

M. Wagner, T. Sawaguchi, G. Kausträter, D. Höffken, G. Eggeler

Structural fatigue of pseudoelastic NiTi shape memory wires

Mater. Sci. Eng., 378 (2004), pp. 105-109

View PDFView articleView in ScopusGoogle Scholar

[10]

S.K. Giri, M. Krishnan, U. Ramamurty

Enhancement of fatigue life of Ni–Ti–Fe shape memory alloys by thermal cycling

Mater. Sci. Eng., 528 (2010), pp. 363-370

View PDFView articleView in ScopusGoogle Scholar

[11]

S. Eucken, T.W. Duerig

The effects of pseudoelastic prestraining on the tensile behaviour and two-way shape memory effect in aged NiTi

Acta Metall., 37 (1989), pp. 2245-2252

View PDFView articleView in ScopusGoogle Scholar

[12]

D. Favier, Y. Liu

Restoration by rapid overheating of thermally stabilised martensite of NiTi shape memory alloys

J. Alloys Compd., 297 (2000), pp. 114-121

View PDFView articleView in ScopusGoogle Scholar

[13]

Y. Liu, D. Favier

Stabilisation of martensite due to shear deformation via variant reorientation in polycrystalline NiTi

Acta Mater., 48 (2000), pp. 3489-3499

View PDFView articleView in ScopusGoogle Scholar

[14]

S. Bagavathiappan, B.B. Lahiri, T. Saravanan, J. Philip, T. Jayakumar

Infrared thermography for condition monitoring - a review

Infrared Phys. Technol., 60 (2013), pp. 35-55

View PDFView articleView in ScopusGoogle Scholar

[15]

Y. Ng, C. Song, D. McLean, S.M. Shimi, T.G. Frank, A. Cuschieri, P.A. Campbell

Optimized deployment of heat-activated surgical staples using thermography

Appl. Phys. Lett., 83 (2003), pp. 1884-1886

View in ScopusGoogle Scholar

[16]

J. Gibkes, W. Siegert, D. Dietzel, I. Delgadillo-Holtfort, B.K. Bein, J. Pelzl

Local influence of material processing on phase transitions in NiTi shape memory alloys investigated by IR thermography

Mater. Sci. Eng., 378 (2004), pp. 175-179

View PDFView articleView in ScopusGoogle Scholar

[17]

D. Favier, H. Louche, P. Schlosser, L. Orgéas, P. Vacher, L. Debove

Homogeneous and heterogeneous deformation mechanisms in an austenitic polycrystalline Ti–50.8 at.% Ni thin tube under tension. Investigation via temperature and strain fields measurements

Acta Mater., 55 (2007), pp. 5310-5322

View PDFView articleView in ScopusGoogle Scholar

[18]

H. Louche, D. Favier, L. Orgéas, V. Delobelle, P. Schlosser

Heat source estimations to study the localized behaviour of superelastic NiTi shape memory alloys

Appl. Imaging Tech. To Mech. Mater. Struct., vol. 4, Springer (2013), pp. 225-228

CrossrefGoogle Scholar

[19]

V. Delobelle, D. Favier, H. Louche

Heat estimation from infrared measurement compared to DSC for austenite to R phase transformation in a NiTi alloy

J. Mater. Eng. Perform., 22 (2013), pp. 1688-1693

CrossrefView in ScopusGoogle Scholar

[20]

S. Gollerthan, M.L. Young, K. Neuking, U. Ramamurty, G. Eggeler

Direct physical evidence for the back-transformation of stress-induced martensite in the vicinity of cracks in pseudoelastic NiTi shape memory alloys

Acta Mater., 57 (2009), pp. 5892-5897

View PDFView articleView in ScopusGoogle Scholar

[21]

Q.P. Sun, H. Zhao, R. Zhou, D. Saletti, H. Yin

Recent advances in spatiotemporal evolution of thermomechanical fields during the solid–solid phase transition

Compt. Rendus Mec., 340 (2012), pp. 349-358

View PDFView articleCrossrefView in ScopusGoogle Scholar

[22]

N. Nayan, D. Roy, V. Buravalla, U. Ramamurty

Unnotched fatigue behavior of an austenitic Ni-Ti shape memory alloy

Mater. Sci. Eng., 497 (2008), pp. 333-340

View PDFView articleView in ScopusGoogle Scholar

[23]

J. Frenzel, E.P. George, A. Dlouhy, C. Somsen, M.F.X. Wagner, G. Eg geler

Influence of Ni on martensitic phase transformations in NiTi shape memory alloys

Acta Mater., 58 (2010), pp. 3444-3458

View PDFView articleView in ScopusGoogle Scholar

[24]

W.S. Choi, E.L. Pang, W.S. Ko, H. Jun, H.J. Bong, C. Kirchlechner, D. Raabe, P.P. Choi

Orientation-dependent plastic deformation mechanisms and competition with stress-induced phase transformation in microscale NiTi

Acta Mater., 208 (2021), p. 116731

View PDFView articleView in ScopusGoogle Scholar

[25]

K. Tanaka, F. Nishimura, M. Matsui, H. Tobushi, P.-H. Lin

Phenomenological analysis of plateaus on stress-strain hysteresis in TiNi shape memory alloy wires

Mech. Mater., 24 (1996), pp. 19-30

View PDFView articleView in ScopusGoogle Scholar

[26]

T.W. Duerig, K.N. Melton, D. Stöckel

Engineering Aspects of Shape Memory Alloys

Butterworth-Heinemann (2013)

Google Scholar

[27]

O.A. Zambrano, R.E. Logé

Dynamic recrystallization study of a Fe-Mn-Si based shape memory alloy in constant and variable thermomechanical conditions

Mater. Char., 152 (2019), pp. 151-161

View PDFView articleView in ScopusGoogle Scholar

[28]

M.J. Donachie, S.J. Donachie

Superalloys: a Technical Guide

ASM international (2002)

Google Scholar

[29]

Y.V.R.K. Prasad, K.P. Rao, S. Sasidhar

Hot Working Guide: a Compendium of Processing Maps

ASM international (2015)

Google Scholar

[30]

S.P. Gadaj, W.K. Nowacki, E.A. Pieczyska

Temperature evolution in deformed shape memory alloy

Infrared Phys. Technol., 43 (2002), pp. 151-155

View PDFView articleView in ScopusGoogle Scholar

[31]

S. Suresh

Fatigue of Materials

Cambridge university press (1998)

Google Scholar

[32]

R.S. Dennis, J.F. Tu

Development of a localized heat treatment system for shape memory alloy wires using an ytterbium fiber laser

J. Mater. Process. Technol., 199 (2008), pp. 245-255

View PDFView articleView in ScopusGoogle Scholar

[33]

C.W. Müller, R. Pfeifer, T. El-
Kashef, C. Hurschler, D. Herzog, M. Oszwald, C. Haasper, C. Krettek, T. Gösling

Electromagnetic induction heating of an orthopaedic nickel–titanium shape memory device

J. Orthop. Res., 28 (2010), pp. 1671-1676

CrossrefView in ScopusGoogle Scholar

[34]

Y. Bellouard

Shape memory alloys for microsystems: a review from a material research perspective

Mater. Sci. Eng., 481 (2008), pp. 582-589

View PDFView articleView in ScopusGoogle Scholar

[35]

G. Costanza, M.E. Tata

Shape memory alloys for aerospace, recent developments, and new applications: a short review

Materials, 13 (2020), p. 1856

CrossrefView in ScopusGoogle Scholar